Chapter 10
Synthesis of Stability Lobe Diagrams

K. Großmann and M. Löser

Abstract. Chatter vibrations during machining lead to poor workpiece surfaces and increased tool wear. In the worst case, the tools and even the main spindle can be damaged. Nowadays, the surface regeneration is considered to be the main effect causing chatter instabilities. Regenerative chatter is initiated by repetitive tooth engagement where the currently engaged tooth cuts the surface produced by the preceding tooth. In a stability lobe diagram (SLD), the stable and unstable areas are separated by the graph of a critical cutting parameter plotted against the spindle speed. Stability lobe diagrams can be used to optimize machining processes in terms of maximizing material removal rate under stable cutting conditions. These SLDs are computed by time domain simulations. However, this consumes a lot of computational time. Thus, several time efficient algorithms in discrete time as well as frequency domain have been developed in the last decades. This chapter scrutinizes under what conditions different algorithms in frequency domain can be applied. The processes are separated regarding cutting conditions and dynamic behavior so that the most time efficient algorithm can be chosen for each class.

10.1 Introduction

To predict the stability boundaries of cutting processes the interactions within the closed-loop of the coupled sub-systems machine and process is examined, Fig. 10.1. Regenerative chatter is caused by the repetitive engagement of a tooth into the surface cut by the preceding tooth. In Fig. 10.1, this is represented by the time delay T.

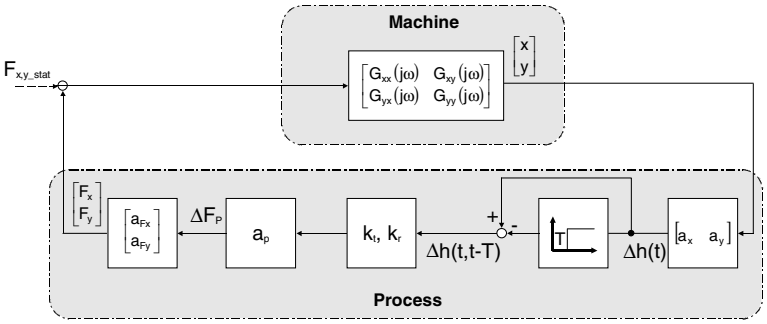

Fig. 10.1 Closed loop of the process-machine interactions [1]

B. Denkena and F. Hollmann (Eds.): Process Machine Interactions, LNPE, pp. 225–244.
springerlink.com

The figure shows an example where the process machine interactions in x-y-plane are investigated and the z direction is neglected. The dynamic behavior of the machine is represented by the transfer function matrix $\mathbf{G}(j\omega)$, which contains the direct transfer functions and the cross transfer functions in x and y direction respectively. However, the process force is a function of chip thickness h. Thus, the deflections in x-y-plane have to be transformed into the direction of chip thickness h. This is conducted by means of so-called directional coefficients (a_x, a_y). With the dynamic chip thickness Δh the dynamic process forces ΔF_p can be computed by applying an empirical cutting force model. Here, this is represented by the tangential coefficient k_t and the radial coefficient k_r. The process forces now have to be transformed into x-y-plane again to close the loop of the process machine interaction.

One method to compute stability boundaries of this closed loop is to model and simulate the interactions in time domain. Modeling non-linearities in the time domain is much easier than in the frequency domain; at the same time, however, the computation time to calculate SLDs increases significantly. One reason for this is that a certain amount of "real time" has to be simulated to ensure the detection of unstable cutting using time signals.

It is more time efficient to analyse the process machine interactions in frequency domain. Analytical methods in frequency domain are the oldest algorithms to predict the stability boundaries and are based on the research works by Tlusty and Polacek as well as by Tobias and Fishwick [2, 3]. Algorithms in frequency domain apply stability criteria like the Nyquist criterion on the open loop transfer function of the process-machine interactions, [1, 4]. In milling operations, the directional coefficients shown in Fig. 10.1 are time-variant and vary periodically with the tooth-passing frequency. To apply the methods in frequency domain average directional coefficients are used. Since the average directional coefficients equal zeroth order Fourier coefficients this method is called zeroth order approximation (ZOA-method).

Operations with highly intermittent cutting conditions, such as low immersion milling, show very strong time variance, which is assumed to affect the process stability. In these cases, the assumption of constant average directional coefficients may lead to incorrect predictions of stability boundaries. Various authors have presented computational time-efficient methods in discrete time domain to determine stability lobe diagrams for highly intermittent cutting operations. Bayly et al. have presented a time-finite element analysis [5], Insperger and Stepan have developed the semi-discretization method [6].

To take the time variant behavior of directional coefficients in frequency domain into account Budak and Altintas expanded their single frequency solution to the multi-frequency solution [7]. This was later on applied to low immersion milling by Merdol and Altintas [8].

Most of the studies that apply these advanced time efficient methods focus on the investigation of single influences (for example: single degree of freedom behavior, helix angle, low immersion milling). In this chapter, the complex influence of different effects is discussed for methods working in frequency domain. ZOA method and two slightly different methods based on the multi-frequency solution

are investigated. The applicability of these methods is scrutinized for a pattern of different cutting conditions and different characteristics of the dynamic machine behavior. The presented works were conducted within a project of the priority program SPP 1180. One goal of the project is to define classification numbers, which allow the selection of an appropriate algorithm before the computation of a stability lobe diagram.

10.2 Computation of SLDs in Frequency Domain

10.2.1 Directed Frequency Response Functions

The open loop transfer function of the process machine interactions can be written as:

$$G_0(j\omega) = a_p \cdot (1 - e^{-j\omega T}) \cdot G_g(i\omega) \tag{10.1}$$

with

T	delay	$T = \frac{1}{n \cdot Z}$
Z	number of teeth	
n	spindle speed	
ω_T	tooth passing frequency	$\omega_T = 2\pi \cdot n \cdot Z$

Here, $G_g(iw)$ is the directed frequency response function. The Nyquist criterion can be applied to this transfer function:

$$\begin{aligned} \mathrm{Re}(G_0(j\omega)) &= \begin{cases} < 1 \text{ stable} \\ = 1 \text{ stability boundary} \\ > 1 \text{ unstable} \end{cases} \\ \mathrm{Im}(G_0(j\omega)) &= 0 \end{aligned} \tag{10.2}$$

Simply spoken, the Nyquist criterion checks if an input signal leaves the open loop without phase shift (imaginary part equals zero) and amplified (real part > 1). Since the output signal is equivalent to the input signal of the subsequent pass through of the loop the signal will be more and more amplified and the closed loop becomes unstable.

In peripheral milling this criterion cannot be applied under any condition since the coordinates in the x-y-plane are coupled, Fig. 10.2. The simplest approach for the solution of this problem is by handling the interaction not in the machine coordinates x and y but by investigating the transfer function at the direction of the chip thickness h. Therefore, the deflections are transformed into the direction of chip thickness and the chip thickness-dependent process forces are transformed back into the direction of the machine coordinates. The transformation is carried out by so-called directional coefficients [1].

Regarding regenerative chatter the static process forces and therefore the static chip thickness can be neglected, [4]. The static chip thickness is the chip thickness that would occur without relative displacements between workpiece and tool. The

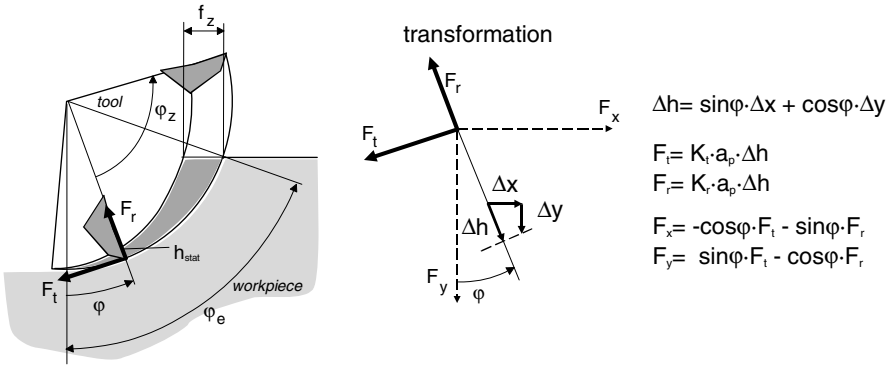

Fig. 10.2 Cutting conditions in peripheral milling

dynamic chip thickness Δh is the change of h caused by the present deflection and the deflection at the time of the preceding tooth engagement.

$$\Delta h = \begin{bmatrix}\sin\varphi & \cos\varphi\end{bmatrix} \cdot \begin{bmatrix}\Delta x \\ \Delta y\end{bmatrix} = \begin{bmatrix}\sin\varphi & \cos\varphi\end{bmatrix} \cdot \left(\begin{bmatrix} x(t) \\ y(t)\end{bmatrix} - \begin{bmatrix} x(t-T) \\ y(t-T)\end{bmatrix} \right) \tag{10.3}$$

Taking into account that the deflections are the reaction of forces acting on the flexible machine structure this can be written in frequency domain.

$$\begin{aligned} \Delta h &= (1 - e^{-j\omega T}) \cdot \begin{bmatrix}\sin\varphi & \cos\varphi\end{bmatrix} \cdot \begin{bmatrix} G_{xx} & G_{xy} \\ G_{yx} & G_{yy}\end{bmatrix} \cdot \begin{bmatrix} F_x \\ F_y\end{bmatrix} \\ \Delta h &= (1 - e^{-j\omega T}) \cdot \begin{bmatrix} a_x & a_y\end{bmatrix} \cdot \begin{bmatrix} G_{xx} & G_{xy} \\ G_{yx} & G_{yy}\end{bmatrix} \cdot \begin{bmatrix} F_x \\ F_y\end{bmatrix} \end{aligned} \tag{10.4}$$

The dynamic process forces are a function of dynamic chip thickness Δh:

$$\begin{bmatrix} F_x \\ F_y\end{bmatrix} = a_p \cdot \begin{bmatrix} -k_t \cdot \cos\varphi - k_r \cdot \sin\varphi \\ k_t \cdot \sin\varphi - k_r \cdot \cos\varphi\end{bmatrix} \cdot \Delta h = a_p \cdot \begin{bmatrix} a_{Fx} \\ a_{Fy}\end{bmatrix} \cdot \Delta h \tag{10.5}$$

Equalizing the vector of process forces in (10.4) with (10.5) and taking the time-delayed re-engagement of the subsequent tooth into account leads to the transfer function of the open loop where G_g denotes the directed frequency response function:

$$\begin{aligned} \mathbf{G}_0 &= a_p \cdot (1 - e^{-j\omega\tau}) \cdot \begin{bmatrix} a_x & a_y\end{bmatrix} \cdot \begin{bmatrix} G_{xx} & G_{xy} \\ G_{yx} & G_{yy}\end{bmatrix} \cdot \begin{bmatrix} a_{Fx} \\ a_{Fy}\end{bmatrix} \\ \mathbf{G}_0 &= a_p \cdot D \cdot \left(a_x a_{Fx} G_{xx} + a_y a_{Fx} G_{yx} + a_x a_{Fy} G_{xy} + a_y a_{Fy} G_{yy} \right) \\ \mathbf{G}_0 &= a_p \cdot D \cdot \left(a_{xx} G_{xx} + a_{xy} G_{yx} + a_{yx} G_{xy} + a_{yy} G_{yy} \right) = a_p \cdot D \cdot G_g \end{aligned} \tag{10.6}$$

The directional coefficients depend on the immersion angle φ and are therefore time-dependent. So, to apply (10.6) in frequency domain average directional coefficients have to be used. Applying the Nyquist criterion and rearranging (10.6) gives the frequency-dependent critical depth of cut a_{pcrit}, [1]

$$a_{pcrit}(\omega) = \frac{-1}{2 \cdot \mathrm{Re}(G_g(j\omega))} \tag{10.7}$$

Since only positive cutting depths are relevant for cutting operations only frequencies with negative real parts of the directed frequency are considered. Furthermore, the relation between chatter frequency and spindle speed can be derived from the Nyquist criterion:

$$n = \frac{60 \cdot f}{z\left(m - \frac{1}{\pi}\arctan\frac{\mathrm{Re}\{G_g(j\omega)\}}{\mathrm{Im}\{G_g(j\omega)\}}\right)} \tag{10.8}$$

With (10.7) and (10.8) the relation between cutting depth and spindle speed and, consequently, the stability lobe diagram (SLD) can be computed. For this purpose, the dynamic behaviour of the machine has to be assumed as constant within the observed range of spindle speed.

(10.7) shows that only frequencies are relevant, whose real parts of the directed frequency response function are negative. For a multi-degree of freedom system (MDoF system) it is possible to divide the directed transfer function G_g into sections, which can be assigned to a specified mode respectively. For each of these sections a mode-dependent stability boundary can be computed. The total stability lobe diagram can now be determined by choosing the minimum of the mode-dependent boundaries at every spindle speed. However, it has to mentioned that this is only valid, if the assumption of averaged directional coefficients can be made and if the directional coefficients are used to compute the directed transfer function G_g as shown in (10.6). The directed transfer function G_g takes the coupling of x and y direction into account. Insperger and Stepan have shown that computing stability lobe diagrams for x and y direction separately by neglecting the geometrical coupling and superposing these SLDs will lead to an incorrect prediction of stability boundaries, [9].

10.2.2 Time Variant Behavior

In milling operations, the directional coefficients are time-variant and vary periodically with the tooth passing frequency. Using average directional coefficients allows a time-efficient computation of the process stability in the frequency domain, as shown in the section before.

As mentioned in the introduction, several authors have introduced computational time-efficient algorithms in discrete time domain to take these effects into account. However, since this chapter deals with the computation of stability in frequency domain the following section focuses on an algorithm based on the multi-frequency solution presented by Altintas and Merdol [8].

Altintas and Merdol [8] utilize the fact that the directional coefficients are periodic with tooth-passing frequency ω_T. Because of this they can be expanded into a Fourier series.

$$a_{xx}(t) = \sum_{r=-\infty}^{\infty} a_{xx,r} \cdot e^{jr\omega_T t}, \quad a_{xx,r} = \frac{1}{T}\int_0^T a_{xx}(t) \cdot e^{-jr\omega_T t} dt \tag{10.9}$$

Taking into account that the relation between time and immersion angle φ is given by the tooth-passing frequency and that the directional coefficients are zero, if the teeth are not engaged, the Fourier coefficients can be written as [8]:

$$a_{xx,r} = \frac{Z}{2\pi}\int_{\varphi_{st}}^{\varphi_{ex}} a_{xx}(\varphi) \cdot e^{-jrZ\varphi} d\varphi \tag{10.10}$$

Where φ_{st} denotes the angle where the teeth engage the workpiece and φ_{ex} denotes the angle where the teeth exit the workpiece. Since the Fourier coefficients of zeroth order are equivalent to the average directional coefficients the methods using average directional coefficients are called zeroth order approximation (ZOA). Fig. 10.3 depicts an example of absolute values of Fourier coefficients.

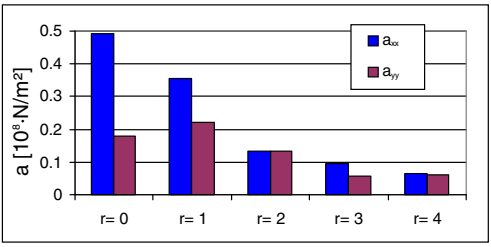

Fourier coefficients of directional coefficients

up milling
d_{tool}= 12 mm
λ= 0°
a_e= 2 mm
number of teeth Z= 4

Fig. 10.3 Example for Absolute Values of Fourier Coefficients

By applying the Fourier series the process forces as a function of the change of the relative deflection between tool and work piece can be written as follows:

$$\mathbf{F}(t) = a_p \cdot \left(\sum_{r=-h_r}^{h_r} \mathbf{A}_r e^{jr\omega_T t} \right) \cdot \Delta\mathbf{x}(t) \tag{10.11}$$

This relation in time domain can be transformed into frequency domain by using the Laplace transformation. The Laplace transforms are given by:

$$\begin{aligned} L\{\Delta x(t)\} &= L\{\mathbf{x}(t) - \mathbf{x}(t-T)\} = \left(1 - e^{j\omega T}\right) \cdot \mathbf{x}(j\omega) = D \cdot \mathbf{x}(j\omega) \\ L\left\{e^{jr\omega_T t} \cdot \mathbf{x}(t)\right\} &= \mathbf{x}\left(j(\omega - r\omega_T)\right) \end{aligned} \tag{10.12}$$

Applying these Laplace transformed is slightly different to the approach introduced in [8] but leads to the same results.

$$\mathbf{F}(\mathrm{j}\omega) = \mathrm{a_p} \cdot \mathrm{D} \cdot \left(\sum_{\mathrm{r}=-\mathrm{h_r}}^{\mathrm{h_r}} \mathbf{A}_\mathrm{r} \cdot \mathbf{x}(\mathrm{j}(\omega - \mathrm{r}\omega_\Gamma)) \right)$$

$$\mathbf{F}(\mathrm{j}\omega) = \mathrm{a_p} \cdot \mathrm{D} \cdot \left(\sum_{\mathrm{r}=-\mathrm{h_r}}^{\mathrm{h_r}} \mathbf{A}_\mathrm{r} \cdot \mathbf{G}(\mathrm{j}(\omega - \mathrm{r}\omega_\Gamma)) \cdot \mathbf{F}(\mathrm{j}(\omega - \mathrm{r}\omega_\Gamma)) \right)$$

$$\mathbf{F}(\mathrm{j}(\omega - \mathrm{p}\omega_\Gamma)) = \mathrm{a_p} \cdot \mathrm{D} \cdot \cdot \left(\sum_{\mathrm{r}=-\mathrm{h_r}}^{\mathrm{h_r}} \mathbf{A}_\mathrm{r} \cdot \mathbf{G}(\mathrm{j}(\omega - (\mathrm{p}+\mathrm{r})\omega_\Gamma)) \cdot \mathbf{F}(\mathrm{j}(\omega - (\mathrm{p}+\mathrm{r})\omega_\Gamma)) \right) \tag{10.13}$$

$$\mathrm{F_p} = \mathrm{a_p} \cdot \mathrm{D} \cdot \left(\sum_{\mathrm{r}=-\mathrm{h_r}}^{\mathrm{h_r}} \mathbf{A}_\mathrm{r} \cdot \mathbf{G}_{\mathrm{p+r}} \cdot \mathbf{F}_{\mathrm{p+r}} \right)$$

For a Fourier order h_r=1 follows:

$$\begin{Bmatrix} \mathbf{F}_{-1} \\ \mathbf{F}_0 \\ \mathbf{F}_1 \end{Bmatrix} = \mathrm{a_p} \cdot \mathrm{D} \cdot \cdot \left(\begin{Bmatrix} \mathbf{A}_{-1} \cdot \mathbf{G}_{-2} \cdot \mathbf{F}_{-2} \\ \mathbf{A}_{-1} \cdot \mathbf{G}_{-1} \cdot \mathbf{F}_{-1} \\ \mathbf{A}_{-1} \cdot \mathbf{G}_0 \cdot \mathbf{F}_0 \end{Bmatrix} + \begin{Bmatrix} \mathbf{A}_0 \cdot \mathbf{G}_{-1} \cdot \mathbf{F}_{-1} \\ \mathbf{A}_0 \cdot \mathbf{G}_0 \cdot \mathbf{F}_0 \\ \mathbf{A}_0 \cdot \mathbf{G}_1 \cdot \mathbf{F}_1 \end{Bmatrix} + \begin{Bmatrix} \mathbf{A}_1 \cdot \mathbf{G}_0 \cdot \mathbf{F}_0 \\ \mathbf{A}_1 \cdot \mathbf{G}_1 \cdot \mathbf{F}_1 \\ \mathbf{A}_1 \cdot \mathbf{G}_2 \cdot \mathbf{F}_2 \end{Bmatrix} \right) \tag{10.14}$$

The right side of (10.14) shows forces $\mathbf{F}$ with indices of $\mathrm{r} = \pm(\mathrm{h_r} + 1)$. Since the absolute values of $\mathbf{A}_\mathrm{r}$ converge to zero for increasing order r the terms with indices of order greater than h_r are set to be zero. It follows:

$$\begin{Bmatrix} \mathrm{F}_{-1} \\ \mathbf{F}_0 \\ \mathbf{F}_1 \end{Bmatrix} = \mathrm{a_p} \cdot \mathrm{D} \cdot \begin{bmatrix} \mathbf{A}_0 & \mathbf{A}_1 & 0 \\ \mathbf{A}_{-1} & \mathbf{A}_0 & \mathbf{A}_1 \\ 0 & \mathbf{A}_{-1} & \mathbf{A}_0 \end{bmatrix} \cdot \begin{bmatrix} \mathbf{G}_{-1} & 0 & 0 \\ 0 & \mathbf{G}_0 & 0 \\ 0 & 0 & \mathbf{G}_1 \end{bmatrix} \cdot \begin{Bmatrix} \mathbf{F}_{-1} \\ \mathbf{F}_0 \\ \mathbf{F}_1 \end{Bmatrix}$$

$$\mathbf{F}^{\mathrm{h}}{}_{\mathrm{out}} = \mathrm{a_p} \cdot \mathrm{D} \cdot \mathbf{A}^{\mathrm{h}} \cdot \mathbf{G}^{\mathrm{h}} \cdot \mathbf{F}^{\mathrm{h}}{}_{\mathrm{in}} \tag{10.15}$$

$$\mathbf{G}_0 = \mathrm{a_p} \cdot \mathrm{D} \cdot \mathbf{A}^{\mathrm{h}} \cdot \mathbf{G}^{\mathrm{h}}$$

This leads to the transfer function of the open loop. Therein, the coordinates are coupled. To apply the Nyquist criterion the investigated system needs only one coordinate or – in the case of a multi variable system – the coordinates have to be decoupled. The coordinates can be decoupled by a modal transformation. The modal coordinates correspond to the eigenvalues of $\mathbf{G}_0$. The Nyquist criterion can now be applied to every one of the $\zeta \cdot (2 \cdot r+1)$ eigenvalues. ζ is the number of the structural coordinates (ζ= 2 for a stability analysis in the x-y-plane), [8].

Since the depth of cut is a scalar value the transfer function can be scaled with a_p.

$$\overline{\mathbf{G}}_0 = \frac{1}{a_p} \cdot \mathbf{G}_0 = \mathrm{eig}\left(\mathrm{D} \cdot \mathbf{A}^{\mathrm{h}} \cdot \mathbf{G}^{\mathrm{h}}\right) \tag{10.16}$$

Fig. 10.4 shows an example of the real and imaginary parts of decoupled transfer functions. In this example, the dynamic behaviour has relevant eigenfrequencies of up to 5 kHz. Since the matrix of transfer functions contains the transfer functions at frequencies shifted by multiples of the tooth passing frequency at a specified frequency, the superposition of transfer functions is periodic with tooth passing frequency. So the stability analysis need not be carried out for the whole bandwidth of 5 kHz but only for a frequency band of the tooth-passing frequency f_t.

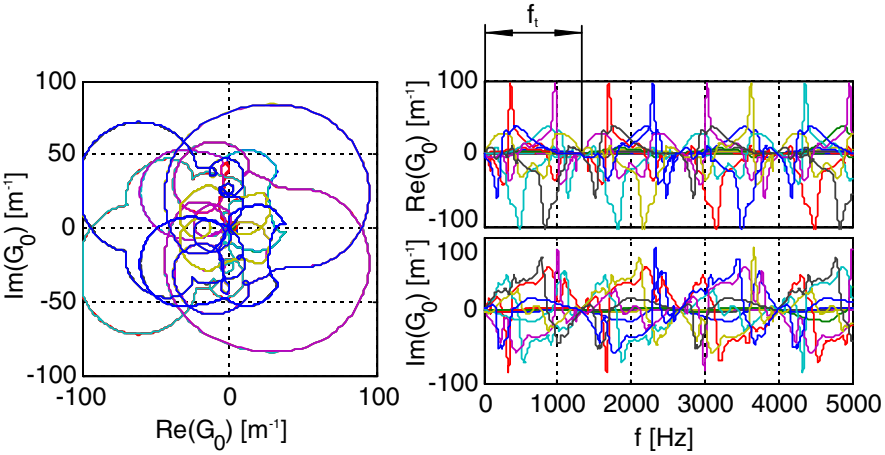

Fig. 10.4 Decoupled and Scaled Transfer Functions of the Open Loop

These sets of transfer functions have to be computed for every discrete spindle the stability boundary has to be determined at. The stability boundaries are given by the reciprocals of the real parts of the intersections between transfer function and real axis. In [10] Altintas et al. assert that "the most conservative and positive depth of cut must be considered as a final solution." So, the critical depth of cut is given by:

$$a_{p\_crit} = \frac{1}{\mathrm{Re}\left(\overline{\mathbf{G}}_0\left(\mathrm{Im}=0\right)\right)_{\max}} \tag{10.17}$$

Fig. 10.5 demonstrates the computation of the stability boundary for the example mentioned before. The relevant parts of the transfer functions are drawn as bold lines and the critical depth of cut is a_{p_crit}= 11.2 mm.

However, the assumption that the critical depth of cut is given by the most conservative real part, is not correct in every case. However, if all intersections with the real axis are analyzed, the algorithm can also be used, if multiple stability boundaries occur at a specified spindle speed. All algorithms in frequency domain

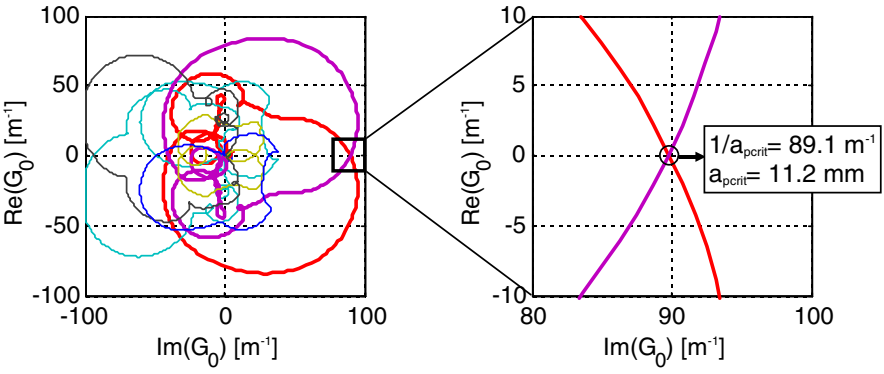

Fig. 10.5 Determination of Critical Depth of Cut

apply the simplified Nyquist criterion shown in (10.2). The complete criterion analyzes not only the intersection of the transfer locus with the real axis. It says the process is stable, if the Nyquist point is encircled counter-clockwise at least once. An intersection with the real axis where the imaginary part changes from positive to negative values will not lead to an unstable process.

Fig. 10.6 shows a simple example to demonstrate this. It depicts a section of a SLD for a one-dimensional process (only x-direction has been taken into account). The dynamic system has an SDoF behavior (m= 0.572 kg; d= 140 Ns/m; c= $2.2 \cdot 10^7$ N/m). The cutting force coefficients are k_t= 3.6·109 N/m² and k_r= 2.25·109 N/m². The figure compares the stability boundaries determined by time domain simulations with the boundaries determined by the multi-frequency solution. The figure also shows the transfer locus for a spindle speed of $n_{spindle}$= 10,600 rpm. Point I marks a counter-clockwise intersection and the process gets unstable at a depth of cut of a_{pcrit}= 7.3 mm. The clockwise intersection at point II compensates the instability and the process becomes stable again up to the depth of cut marked by point III.

10.2.3 Cutting-Depth-Dependent Behavior

Not only the radial immersion has an influence on the "smoothness" of the cutting forces. An increasing helix angle will cause forces that change less rapidly over time. Assuming the parameters of the process force model are unaffected by the helix angle, the average forces – i. e. the zeroth order Fourier coefficients - are also independent from the helix angle. However, the higher order Fourier coefficients are influenced by the helix angle. This can be illustrated by the process forces.

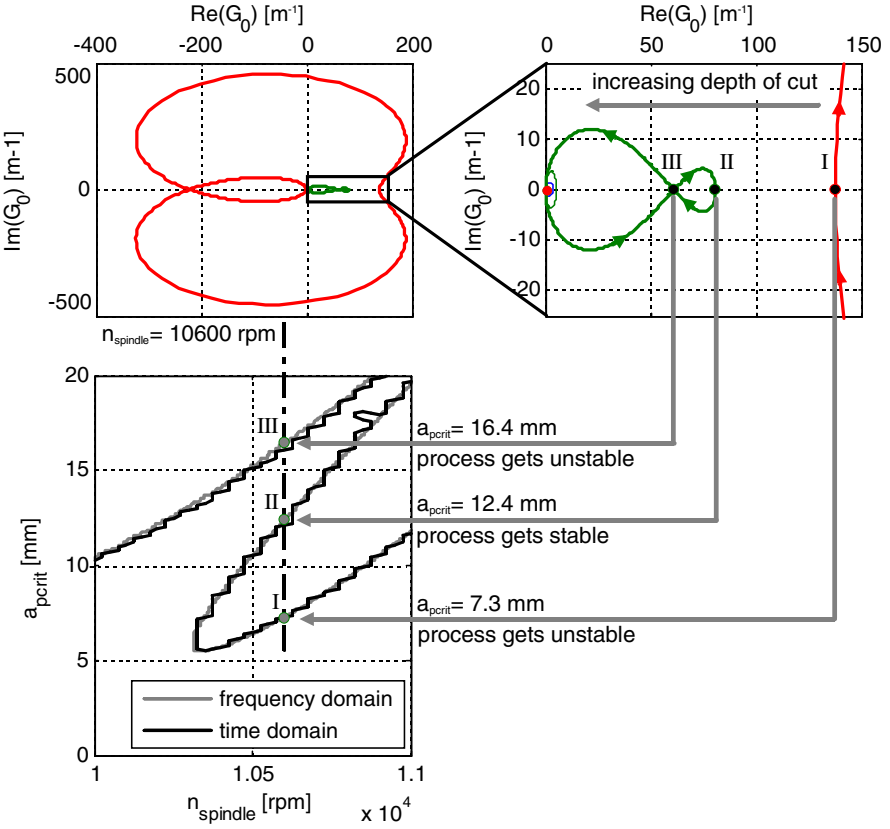

Fig. 10.6 Multiple Stability Boundaries at one Spindle Speed

Fig. 10.7 shows simulated process forces F_y for different helix angles at axial cutting depths a_p= 10 mm and a_p= 20 mm but in both cases for the same radial depth of cut a_e= 3mm. The figure also depicts the spectra of the process forces. For the straight fluted mill there is a sharp change of the forces when the cutting edge leaves the workpiece. The force at zero frequency (which equals the average force) is independent of the helix angle. The forces at the tooth-passing frequency and their harmonics decrease with increasing helix angle. The decreasing effect is more significant for the axial depth of cut of a_p= 20 mm.

The magnitudes of the process forces at tooth-passing frequency and their harmonics correspond to the Fourier coefficients. Thus, for helicoidal mills the values of the Fourier coefficients depend on the axial depth of cut a_p. In this case, the value of the Fourier coefficients is given by [11]:

$$\mathbf{A}_r^* = \mathbf{A}_r \cdot \frac{1 - e^{-j \cdot r \cdot 2 \cdot \pi \cdot a_p / p}}{j \cdot r \cdot 2 \cdot \pi \cdot a_p / p} \tag{10.18}$$

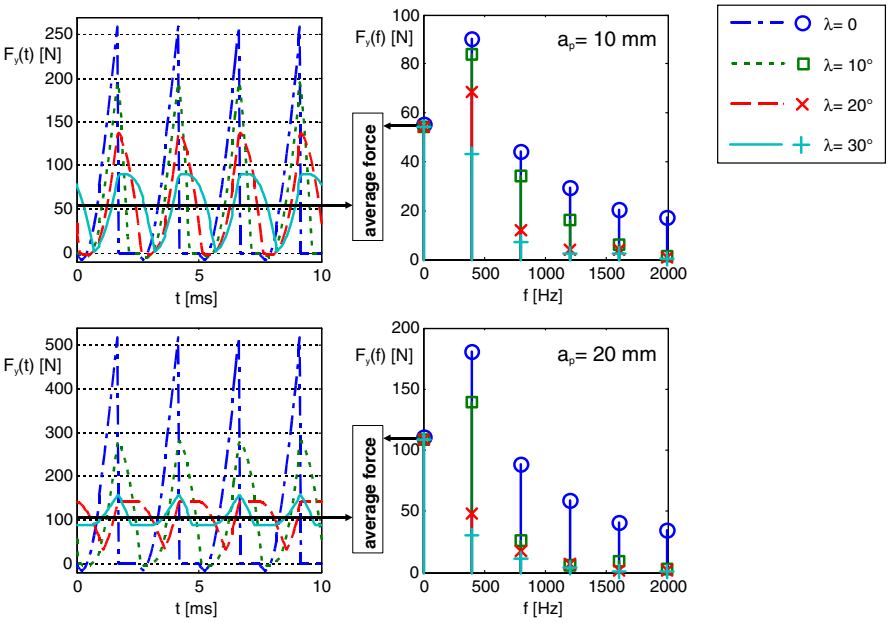

Fig. 10.7 Process Forces and Spectra of Process Forces

A_r represents the Fourier coefficients for the straight-fluted mill and p is the pitch of a tool with Z teeth.

$$p = \frac{d_{Tool} \cdot \pi}{Z \cdot \tan(\lambda)} \tag{10.19}$$

With increasing axial depth of cut the values of the Fourier coefficients decrease. The Fourier coefficients differ for the different helix angles. The zeroth order coefficients are independent of the helix angle but the values of the higher order coefficient decrease with an increasing helix angle λ.

Similar to (10.15), the open loop transfer function can be written as follows:

$$\mathbf{G}_0 = a_p \cdot D \cdot \mathbf{A}^{*h} \cdot \mathbf{G}^h \tag{10.20}$$

Decoupling the coordinates in (10.20) and applying the Nyquist criterion could still be carried out by computing the eigenvalues, as described in the chapter before. This can be achieved by computing the eigenvalues for the characteristic equation

$$\det\left[\mathbf{I} + \Lambda \mathbf{A}^h \mathbf{G}^h\right] = 0 \tag{10.21}$$

with $\Lambda = a_p\left(1 - e^{j\omega T}\right)$, [8].

However, if the decoupled system has to be computed for every a_p, it is less time consuming to apply a different approach. For a multi-variable system the stability analysis can be carried out for the determinant of the matrix of open loop transfer functions minus identity matrix:

$$\overline{\mathbf{G}}_0 = \det\left|\mathbf{G}_0 - \mathbf{I}\right| \tag{10.22}$$

The behavior of the whole system is therefore summarized in a transfer function for a single coordinate. The open loop is stable, if the transfer function does not encircle the point {0, 0·i}. This way, the determination of stability boundaries is numerically easier, especially for a Fourier series expansion of higher order.

Since the elements of matrix of Fourier coefficients $\mathbf{A}^{*h}$ depend on the axial depth of cut the transfer function cannot be scaled with a_p as described by (10.16). Thus, applying the Nyquist criterion only provides information, if a specified combination of spindle speed and axial depth of cut results in a stable process or not. A change of axial depth of cut a_p leads to different transfer locuses and the stability boundary at a given spindle speed has to be determined iteratively. In the following sections, the above-described algorithm is called Multifreq_det algorithm.

10.2.4 Summary

In the previous three sections, different algorithms for the computation of stability lobe diagrams have been shown. The first and simplest one is the well-known zeroths order approximation (ZOA). The last two approaches are expanded versions of the multi-frequency solution presented by Merdol and Altintas. One of them uses the computation of eigenvalues to decouple the system of multiple "frequency coordinates" (Multifreq_eig) and the other one computes the determinants of the transfer matrices (Multifreq_det). Which algorithm is best suitable for the determination of a SLD depends on the effects that have to be taken into account. However, the more complex the algorithm gets, the more computational time is needed. But even the algorithm for a depth-of-cut-dependent behavior is less time-consuming than time domain simulations. In the following section, these algorithms are applied to cutting operations with different process and machine behavior.

10.3 Application

10.3.1 Models of Process and Machine

The following investigations use the example of an up-milling operation with cylindrical end mills. Table 10.1 shows the parameters of this reference process as

well as the coefficients of the process force model. To describe the process forces a linear force model was used [12]. The parameters were conducted by means of cutting tests for aluminium AA7075 workpieces.

Table 10.1 Parameters of the Reference Process

Process		Up-milling
Tool	Number of teeth	Z= 4
	Tool diameter	d_{Tool}= 12 mm
Workpiece	Material	AlZn5,5MgCu (AA7075)
	Tangential force coefficient	k_t= 830 N/mm²
	Radial force coefficient	k_r= 225 N/mm²

The dynamic behavior is represented by modal models. The parameters of these models have been identified from measured frequency response functions of different spindle tool systems. In all cases, cross compliances have been neglected. The frequency response functions are therefore computed as follows:

$$\begin{aligned} G_{xx} &= \sum_{m=1}^{n_x} \frac{1}{-m_{x,m}\omega^2 + j\omega d_{x,m} + c_{x,m}} \\ G_{yy} &= \sum_{m=1}^{n_y} \frac{1}{-m_{y,m}\omega^2 + j\omega d_{y,m} + c_{y,m}} \\ G_{xy} &= G_{yx} = 0 \end{aligned} \tag{10.23}$$

with number of eigenmodes n, the modal parameters mass m, damping d and stiffness c.

10.3.2 Rotational Symmetric SDoF System

The single degree of freedom system is meant here as the single degree of freedom behavior in the x and y-directions respectively. Such a behavior with just one dominant eigenfrequency is typical for tools with a large length-to-diameter ratio. Fig. 10.8 shows the measured frequency response function of a carbide dummy tool with a ratio of l/d= 8. It shows a dominant eigenfrequency at 728 Hz. The response functions are nearly the same for x and y- direction. The modal parameters identified from the measured data and used for the computation of stability lobe diagrams are shown in Table 10.2.

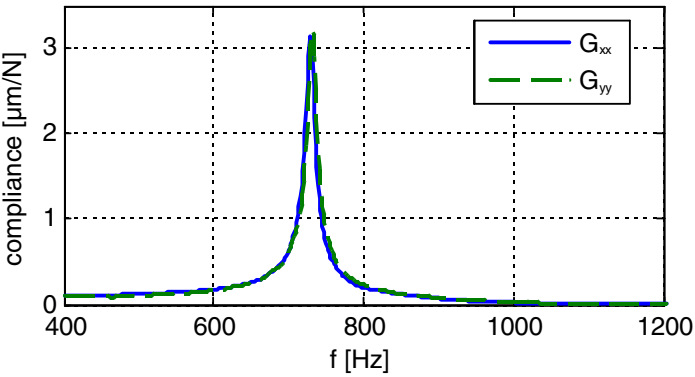

Fig. 10.8 Reference for a SDoF Behavior

Table 10.2 Modal Parameters of the SDoF System

	G_{xx}	G_{yy}
Mass m [kg]	0.922	0.925
Damping d [kg/s]	69	69
Stiffness c [N/m]	$1.93 \cdot 10^7$	$1.95 \cdot 10^7$

For the example of SDoF, several authors showed systems that may occur at small radial immersion additional stability lobes. These additional stability lobes cannot be predicted by the ZOA-method. Zatarain et al. [11] investigated the influence of the helix angle on chatter stability by using the multi-frequency solution by Merdol and Altintas as well as the semi-discretization method by Insperger and Stepan. This work showed that for increasing helix angles the additional lobes transform into closed instability islands. The same behavior can be shown for this example here.

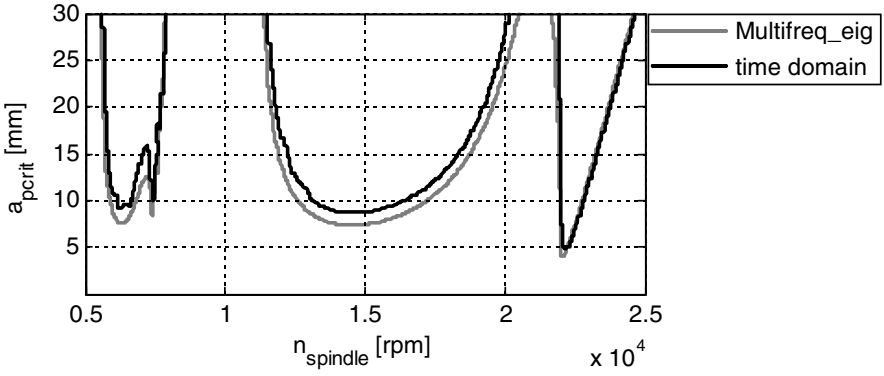

Fig 10.9 SLDs of the SDoF System, $\lambda = 0°$, $a_e = 0.5$ mm

Fig. 10.9 shows a comparison of SLDs computed by time domain simulation and by the Multifreq_eig algorithm. The time domain and the frequency domain solution are in good agreement and show the additional stability lobes.

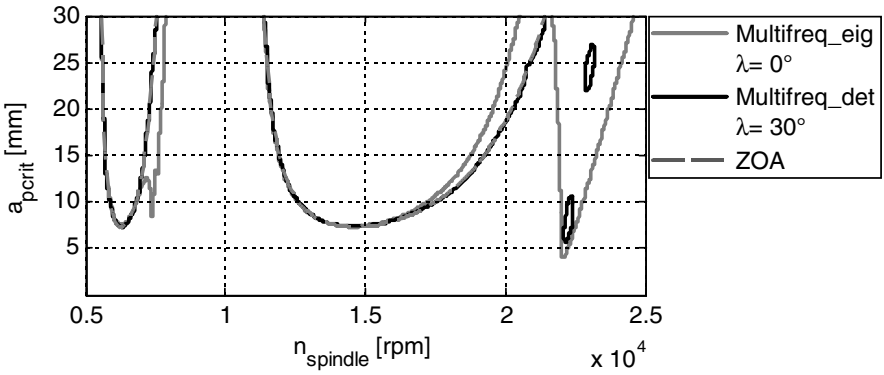

Fig. 10.10 SLDs of the SDoF System, a_e= 0.5 mm

With increasing helix angle, the additional stability lobes transform into unstable islands within the stable area. This can be shown with the multi-frequency solution as well as by time domain simulations. Since the directional coefficients depend on depth of cut the Multifreq_det algorithm has to be used in the case of a helix angle λ= 30°. For a helix angle of λ= 0 the Multifreq_eig algorithm is used. For a helix angle of λ= 30° the ZOA algorithm shows nearly the same results as the multi-frequency solution, except the unstable islands, Fig. 10.10.

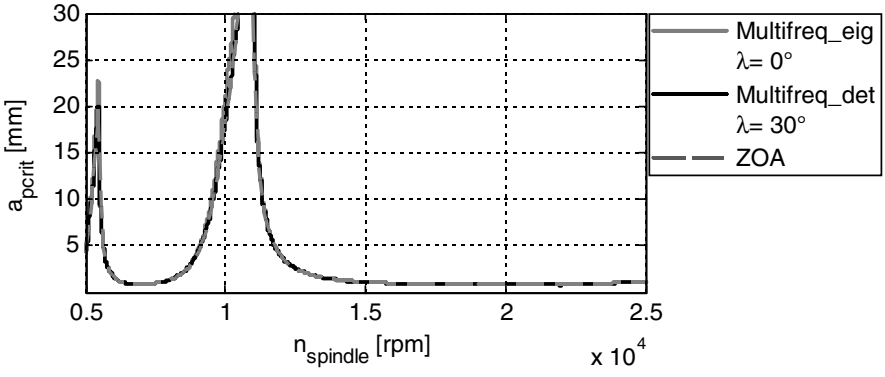

Fig. 10.11 SLDs of the SDoF System ae= 3 mm

For larger radial immersions the time variant behavior of the directional coefficients gains less impact on the stability boundaries. At a radial depth of cut of a_e= 3 mm, no impact of the helix angle can be shown and the ZOA algorithm results in practically identical stability boundaries to the multi-frequency solution,

Fig. 10.11. In this case, the fast ZOA method can be applied without loosing accuracy of the predicted stability boundaries.

10.3.3 Rotational Symmetric MDoF System

As shown in the example, in the previous chapter the dynamic behavior of spindle tool systems with long slender tools is dominated by the eigenmodes of the free projecting part of the tool. Tools with a lesser length-to-diameter ratio eigenmodes of the spindle and the spindle stock gain more impact on the dynamic behavior at the tool centre point (TCP). This results in the behavior of a multi-degree of freedom system (MDoF System) with several modes that may cause chatter instability.

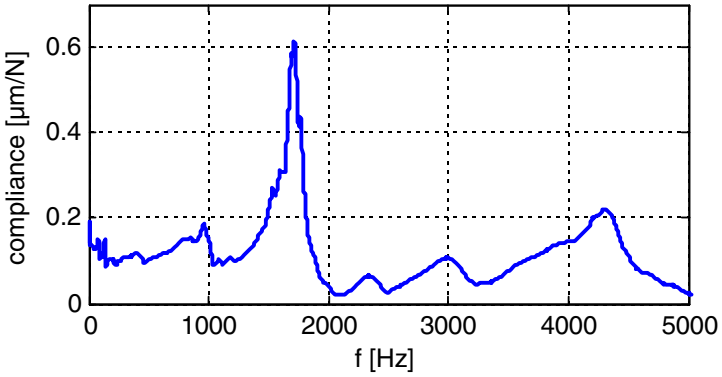

Fig. 10.12 Dynamic Behavior of the Rotational Symmetric MDoF System

Fig. 10.12 depicts a frequency response function in y-direction measured at a tool with a length-to-diameter ratio of l/d=2.5. Assuming a rotational symmetric system, the frequency response function in x-direction is set to be equal to the response function in y-direction.

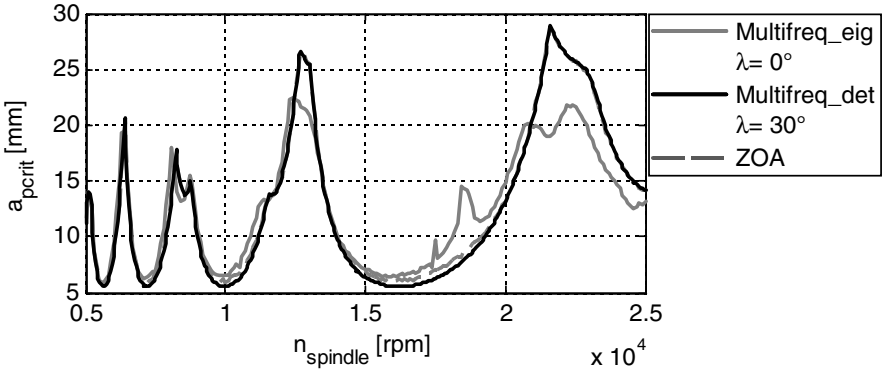

Fig. 10.13 SLDs of the Symmetric MDoF System, a_e= 3 mm

The investigated SDoF system has no impact on the stability boundaries at a radial depth of cut of a_e= 3 mm. This is different for the symmetric MDoF system. For the straight-fluted mill an impact on the stability can be seen around the spindle speed of about 20,000 rpm. However, for a helix angle of λ= 30° the multi-frequency solution is in good agreement with the stability boundaries obtained by the ZOA method, Fig 10.13. An increase of the radial depth of cut will minimize the impact of the time-variant directional coefficients even for the straight-fluted mill, Fig. 10.14.

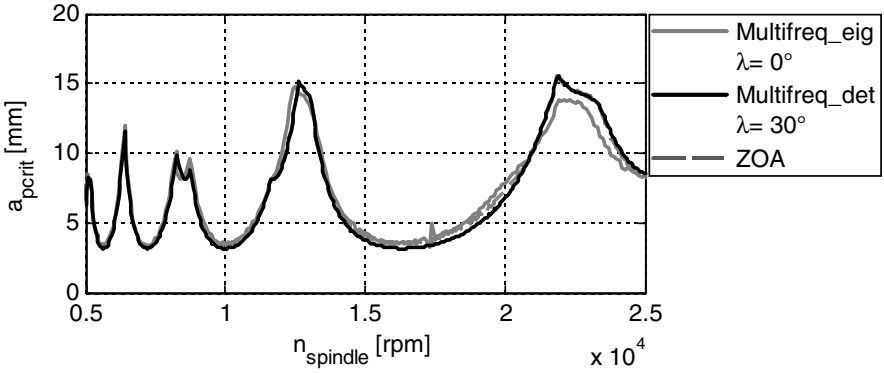

Fig. 10.14 SLDs of the Symmetric MDoF System, a_e= 5 mm

10.3.4 Non-rotational Symmetric MDoF System

Usually spindle and milling tool are rotational symmetric systems. In most cases, however, the spindle stock is non-rotationally symmetric. Especially for tools with a small length-to-diameter ratio this may have an impact on the dynamic behavior at the tool centre point. In addition to Fig. 10.12, Fig. 10.15 shows the measured frequency response functions in x and y-direction. The response functions differ for the different directions.

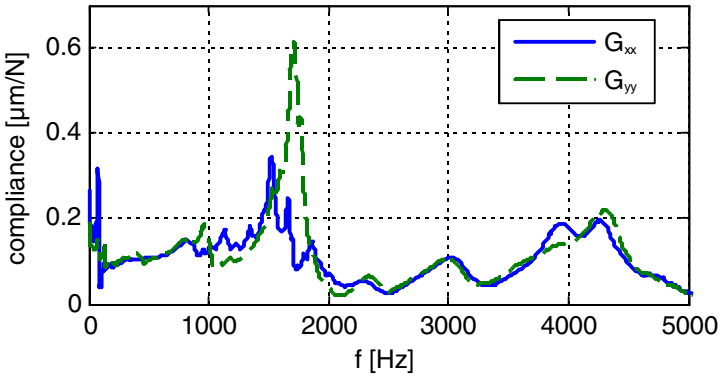

Fig. 10.15 Dynamic Behavior of the Non-Symmetric MDoF System

Fig. 10.16 and Fig. 10.17 show a comparison of the SLDs computed by multi-frequency solution and ZOA method for radial immersions a_e= 3 mm and a_e= 5 mm respectively. In both cases, the ZOA method provides acceptable results for a helix angle of λ= 30°. However, compared with the results for the symmetric system the zero helix angle also has an impact at higher radial immersions.

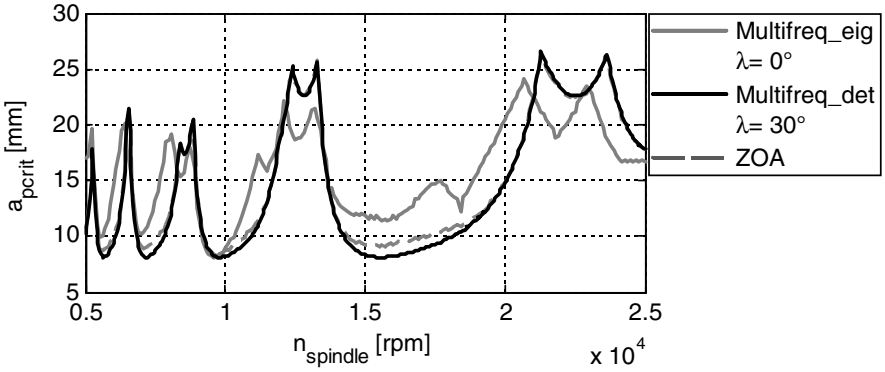

Fig. 10.16 SLDs of the Non-Symmetric MDoF System, a_e= 3 mm

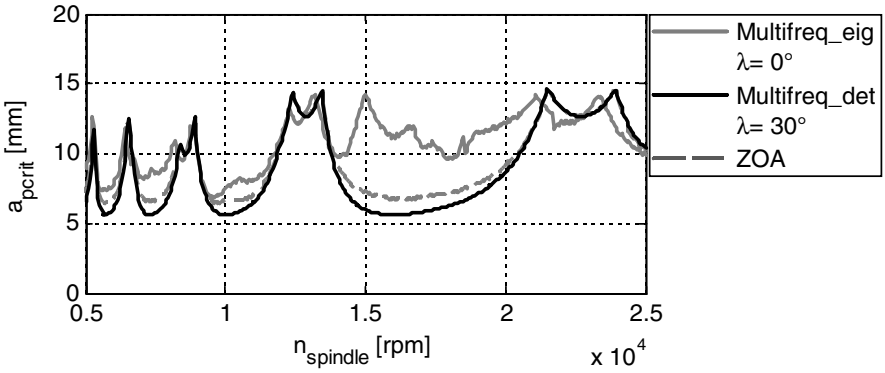

Fig. 10.17 SLDs for the Non-Symmetric MDoF System, a_e= 5 mm

10.4 Conclusions

The behavior of the mechanical system in combination with the process behavior has an impact on the stability. This means that the process and machine behavior determines which effects have to be taken into account for an accurate prediction of stability boundaries.

In a case study - presented in this chapter - algorithms for the prediction of stability boundaries in frequency domain have been applied to different combinations of process and machine characteristics. A comparison with results in time domain

has demonstrated that frequency domain algorithms are applicable, even if the system shows a time-variant behavior. It has been demonstrated that in some cases a simplification can be made so that the time efficient zeroth order approximation is applicable. Table 10.3 shows a pattern of the computational methods for the investigated combinations of process and machine behavior.

Table 10.3 Pattern of Applicable Frequency Domain Algorithms for the Investigated Reference Process

	Symmetric SDoF	Symmetric MDoF	Non-Symmetric MDoF
Straight-fluted $a_e / d \approx 0.04$	Multifreq eig	Multifreq eig	Multifreq eig
Helicoidal $a_e / d \approx 0.04$	Multifreq det	Multifreq det	Multifreq det
Straight-fluted $a_e / d \approx 0.25$	ZOA	Multifreq eig	Multifreq eig
Helicoidal $a_e / d \approx 0.25$	ZOA	ZOA	ZOA
Straight-fluted $a_e / d \approx 0.4$	ZOA	ZOA	Multifreq eig
Helicoidal $a_e / d \approx 0.4$	ZOA	ZOA	ZOA

This pattern is valid for the investigated reference process. Ongoing works deal with the definition of classification numbers to expand this pattern for a general process and machine behavior. Some investigated issues that have to be quantified are, for example, the influence of tool diameter and cutting force coefficient as well as the quantification of the influence of the dynamic behavior, i. e. number of modes and dynamic stiffness.

References

[1] Weck, M., Brecher, C.: Werkzeugmaschinen Fertigungssysteme Bd.5 Messtechnische Untersuchung und Beurteilung, dynamische Stabilität. Springer, Heidelberg (2006)

[2] Tlusty, J., Polacek, A.: Beispiele der Behandlung der selbsterregten Schwingungen der Werkzeugmaschinen, 3. Forschungs- und Konstruktionskolloquium Werkzeugmaschinen und Betriebswissenschaft (3. FoKoMa). Vogel-Verlag, Coburg (1957)
[3] Tobias, S.A., Fishwick, W.: A Theory of Regenerative Chatter. The Engineer, London (1958)
[4] Altintas, Y., Budak, E.: Analytical Prediction of Stability Lobes in Milling. Annals of the CIRP 44(1), 357–362 (1995)
[5] Bayly, P.V., Halley, J.E., Mann, B.P., Davies, M.A.: Stability of Interrupted Cutting by Temporal Finite Element Analysis. Journal of Manufacturing Science and Engineering 125, 220–225 (2003)
[6] Insperger, T., Stepan, G.: Semi-discretization method for delayed systems. International Journal for Numerical Methods in Engineering 55, 503–518 (2002)
[7] Budak, E., Altintas, Y.: Analytical Prediction of Chatter Stability in Milling. Part I: Modelling, Part II: Applications, Transactions of ASME, Journal of Dynamic Systems, Measurement and Control 120, 22–36 (1998)
[8] Merdol, S.D., Altintas, Y.: Multi Frequency Solution of Chatter Stability for Low Immersion Milling. ASME Journal of Manufacturing Science and Engineering 126, 459–466 (2004)
[9] Insperger, T., Stepan, G.: Stability Transition between 1 and 2 Degree-of-Freedom Models of Milling. Periodica Polytechnica Mechanical Engineering 48(1), 27–39 (2004)
[10] Altintas, Y., Stepan, G., Merdol, D., Dombovari, Z.: Chatter stability of milling in frequency and discrete time domain. CIRP Journal of Manufacturing Science and Technology 1, 35–44 (2008)
[11] Zatarain, M., Munoa, J., Peigne, G., Insperger, T.: Analysis of the Influence of Mill Helix Angle on Chatter Stability. Annals of the CIRP 55(1), 365–368 (2006)
[12] Altintas, Y.: Modeling Approaches and Software for Predicting the Performance of Milling Operations at MAL-UBC. Machining Science and Technology 4(4), 445–478